# Fast Motion, the Initial Drop and the Onset of Friction

Kit Gallagher
Supervisor: Dr David Ward

Summer 2020

**Abstract**

The motion line-shape in the intermediate scattering function, particularly in the ballistic region, is considered for the Li/ Cu (111) system. The effect of varying environmental parameters is demonstrated on particle trajectories, and the resulting ISFs were in agreement with the analytic lineshapes. When fitting the ballistic ISF to a general Gaussian, the wavevector $\mathbf{K}$ and the inverse of the standard deviation $\sigma$ are shown to be directly proportional, in agreement with 2D ideal gas law. While traditional analysis methods rely on the central limit theorem, so the experimental noise spectrum need not be consistent with that used in Langevin simulations, a coloured noise approach is used here to better replicate the physical impulse spectrum experienced by the adatoms. In conjunction with a potential energy surface, this is used to produce simulations in wider agreement with existing experimental measurements of this system, into the short-time ballistic region.

## 1 Introduction

Helium-3 surface spin echo (HeSE) is an inelastic scattering technique in surface science that has been used to measure microscopic dynamics at well-defined surfaces in ultra-high vacuum [1]. Spin polarised Helium-3 wavepackets are manipulated by magnetic fields via interactions with the nuclear magnetic moment. Wavepackets are split by spin state, with the final beam polarisation being proportional to the intermediate scattering function considered throughout this report.

The information available from HeSE complements and extends that available from other inelastic scattering techniques such as neutron spin echo and traditional helium-4 atom scattering (HAS). 3HeSE technique is particularly appropriate for measuring adsorbate dynamics at surfaces, as it provides surface correlation measurements in the picosecond to nanosecond time range [2].

These techniques can be applied in the development of heterogeneous catalysts and semiconductor structures, which may be limited by the mass-transport step controlled by adatom surface diffusion [3]. Alkali metals adsorbed on metal surfaces are of particular technological relevance due to the ability of the adsorbate to modify the electronic structure of the surface and its resultant chemical properties [4, 5].

While such surface dynamics can be modelled through the popular Monte Carlo approach [6, 7], this is costly and inefficient. An alternative is to use Langevin equation based molecular dynamics (MD) simulations [8], where the interaction of adsorbates with the substrate atoms is described using a frozen potential energy surface (PES), a drag term and a stochastic fluctuating force.

The effect of coloured noise on particle trajectories is described by the Generalised Langevin Equation (GLE) in Section 2.3. This is modelled using the PIGLE software [9], described in section 3.1, and contrasted to experimental data of Li on a Cu(111) surface from X. All simulations at baseline parameters $m = 7amu, T = 140K, \eta = 5ps^{-1}$, with no inter-particle interactions, unless otherwise stated.

# 2 Theoretical Background

## 2.1 Scattering

Let us consider helium atoms incident on the sample, that are subsequently scattered off in a direction. The important quantity for our scattering experiments is the momentum transfer parallel to the surface, given by

$$\mathbf{\Delta K} = K_i[sin(\delta - \gamma) - sin(\gamma)] \tag{1}$$

where $\gamma$ is the angle of incidence on the surface and $\delta$ is the total scattering angle. The $\mathbf{K}$ vector defines the azimuth on the crystal surface that is considered for scattering.

We use a simple kinematic scattering model, where the scattered amplitude is given by

$$A = F \times S \tag{2}$$

$F$ is the form factor for scattering, which depends on the shape of the scatterer, and determines the spatial distribution of scattered intensity. In general, we do not know the form of $F$ nor how it depends on $\mathbf{\Delta K}$, so it is taken as unity.

$S$ denotes the structure factor, dependant on the atomic positions. This can be described by:

$$S = e^{-i\mathbf{\Delta K}\cdot\mathbf{r}} \tag{3}$$

This gives a complex expression for the scattered amplitude:

$$A(\mathbf{\Delta K}, t) = e^{-i\mathbf{\Delta K}\cdot\mathbf{r}(t)} \tag{4}$$

The observable quantity in the spin-echo experiment is the Intermediate Scattering Function (ISF),

which is the autocorrelation of the time-dependent amplitude, A(t). From the Wiener–Khinchin theorem, the autocorrelation can be computed through application of the fast Fourier Transform of A(t), and inverse transforming the modulus squared of the transform [10].

### 2.2 Langevin Equation

Before consideration of the GLE, it is instructive to first consider the Langevin Equation (LE) which is commonly used to describe surface diffusion. The original Langevin Equation [11] describes Brownian motion, the random movement of microscopic particles in a fluid due to collisions with molecules of the surrounding medium, however can also be applied to the diffusion of adsorbate molecules across a surface. The LE can be expressed as:

$$m\frac{d\mathbf{v}}{dt} = -\lambda\mathbf{v} + \boldsymbol{\xi}(t) \tag{5}$$

where $m$ is the mass of the particle in question, and $\mathbf{v}$ is its velocity. The force acting on the particle is written as a sum of a viscous force $-\lambda m\mathbf{v}$ proportional to the particle's velocity (given by Stokes' law [12]), and a stochastic noise term $\boldsymbol{\xi}(t)$. In multi-species systems, the viscous/friction coefficient $\lambda$ may be dependant on the identity of the adsorbate species (adatom), however we will only consider single-species systems in this report.

This may be extended further through consideration of an external (position dependant) potential $V$ and an inter-particle interaction force $\mathbf{F}_{ij}$ between adatoms $i$ and $j$.

$$m\frac{d\mathbf{v}_i}{dt} = -\nabla V - m\lambda\mathbf{v}_i + \boldsymbol{\xi}(t) + \Sigma_{j\neq i}\mathbf{F}_{ij} \tag{6}$$

It should be noted that the substrate may only be replaced with a frozen potential $V(r)$ (described as the Potential Energy Surface or PES) if the timescale of the adsorbate motion is much smaller than that of the substrate atoms, so the substrate's degrees of freedom are separated from those of the adsorbate.

The stochastic force $\boldsymbol{\xi}(t)$ follows a Gaussian probability distribution with zero mean and the correlation function:

$$\left\langle \xi_i(t)\xi_j(t')\right\rangle = 2m\lambda k_B T\delta_{i,j}\delta(t-t') \tag{7}$$

where $k_B$ is Boltzmann's constant, $T$ is the temperature, and $\eta_i$ is the i-th component of the vector $\boldsymbol{\eta}$. The angle brackets refer to the inverse Fourier transform of the power spectrum, which defines an autocorrelation function according to the Wiener–Khinchin theorem [13]. The use of $\delta$-functions assumes that the force at any time $t$ is completely uncorrelated with any other time, which is valid for the motion of a macroscopic particle at sufficiently large time scales.

### 2.3 Generalised Langevin Equation

However, at short time scales, the LE breaks down as the stochastic force can no longer be considered random; in the example of Brownian motion this occurs when the time scale of the molecular motion is no much less than that of the motion of the particle under observation. Crucially this means the auto correlation of the stochastic force between different points in time is no longer zero; i.e. we cannot assume (7) for a random force.

The GLE (given below) combines friction and stochastic terms, and is used to describe this non-Markovian processes, where a complete history of a particles motion is required to predict future motion analytically (as opposed to a Markovian process, where only information on the current state is required [14]).

$$m\frac{d\mathbf{v}_i}{dt} = -\nabla V - m\int_{-\infty}^{t} \lambda(t-t')\mathbf{v}_i(t')dt' + \boldsymbol{\zeta}(t) + \Sigma_{j\neq i}\mathbf{F}_{ij} \tag{8}$$

Damping in the form of the memory function $\lambda(t-t')$ and the fluctuating force $\boldsymbol{\zeta}(t)$ are not independent since they both arise from the coupling to the substrate. These quantities are related by the second Fluctuation-Dissipation theorem [15], where the conservation of temperature requires that $\boldsymbol{\zeta}$ still has zero mean, and must satisfy:

$$\left\langle \zeta_i(t)\zeta_j(t')\right\rangle = 2mk_BT\delta_{i,j}\lambda(t-t') \tag{9}$$

As stated above, for the GLE, the auto-correlation function of the stochastic force may now be non-zero when $t \neq t'$, unlike in (7) for the LE. Such noise sources are commonly referred to as 'coloured noise', due to the frequency dependence of the Fourier transform of $\lambda(t-t')$.

### 2.4 LE Intermediate Scattering Function

As the ISF is the experimentally measured quantity in HeSE (derived from polarisation), it is instructive to consider this further. While the ISF is defined from the scattering amplitude, it can also be determined directly from the particle's trajectory [16]:

$$I(\mathbf{K},t) = \langle e^{-i\mathbf{K}[\mathbf{R}(t)-\mathbf{R}(0)]}\rangle = \langle e^{-i\mathbf{K}\int_0^t v_{\mathbf{K}}(t')dt'}\rangle \tag{10}$$

where $v_{\mathbf{K}}$ is the velocity of the adparticle projected along the direction of the wavevector $\mathbf{K}$. According to the Chudley-Elliot model [17], this can further be written as:

$$I(\mathbf{K},t) = e^{-\mathbf{K}^2\int_0^t (t-t')\langle v_{\mathbf{K}}(t')v_{\mathbf{K}}(0)\rangle dt'} \tag{11}$$

when the thermal noise is Gaussian white noise and there is no interaction potential or it is

quadratic. If a stochastic process is Gaussian and Markovian, Doob's theorem [18] states that its correlation function decays in time exponentially. If we assume simply

$$\langle v_{\mathbf{K}}(t)v_{\mathbf{K}}(0)\rangle = \langle v_{\mathbf{K}}^2\rangle e^{-\frac{t}{\tau_c}} \tag{12}$$

where $\tau_c$ is the (normalized) correlation time for the adparticle velocity:

$$\tau_c = \frac{1}{\langle v_{\mathbf{K}}^2\rangle}\int_0^\infty \langle v_{\mathbf{K}}(t)v_{\mathbf{K}}(0)\rangle dt \tag{13}$$

This means that the intermediate scattering function can be expressed as [19]:

$$I(\mathbf{K},t) = exp\left[-\chi^2\left(e^{-\frac{t}{\tau_c}} + \frac{t}{\tau_c} - 1\right)\right] \tag{14}$$

where

$$\chi = \tau_c\sqrt{\langle v_{\mathbf{K}}^2\rangle}|\mathbf{K}| = \frac{D|\mathbf{K}|}{\sqrt{\langle v_{\mathbf{K}}^2\rangle}} = \bar{l}|\mathbf{K}| \tag{15}$$

in which $D$ is the diffusion coefficient, and $\bar{l}$ is the mean free path. Note that, in the short time limit $t < \tau_c$, we may approximate the ISF to have a Gaussian form:

$$I(\mathbf{K},t) \propto e^{\frac{-D|\mathbf{K}|^2t^2}{2\tau_c}} \tag{16}$$

### 2.5 GLE Intermediate Scattering Function

It is also possible to consider an analytic form for the ISF in the case of the GLE, provided again that there is no potential surface. This is derived by Townsend et al. [20], and only their results will be replicated here.

The closed form is written as $I(\Delta K,t) = exp[-\Delta K^2 X(t)]$, where $X(t)$ is given by:

$$X(t) = \frac{k_BT}{m\lambda^2}\left(\frac{\lambda}{\omega_c} - 1 + \lambda t + \frac{e^{-\omega_c t/2}}{\omega_c}\left[C\cosh\omega t + S\sinh\omega t\right]\right) \tag{17}$$

with the coefficients S and C given by:

$$C = \omega_c - \lambda, \qquad S = \frac{\sqrt{\omega_c}(\omega_c - 3\lambda)}{\sqrt{\omega_c - 4\lambda}} \tag{18}$$

and the frequency scale $\omega$ combines the two basic frequency scales of the problem, $\omega_c$ and $\lambda$, by:

$$\omega = \frac{1}{2}\sqrt{\omega_c^2 - 4\lambda\omega_c} \tag{19}$$

Note that $\omega$ becomes complex unless the cut-off frequency $\omega_c$ is at least four times faster than the strength of friction $\lambda$, while the classical ISF remains real at all times.

This is in agreement with a generalised treatment of the Chudley-Elliot model [21], which associates $\omega$ which the frequency of the frustrated translational mode (or T mode), the lowest frequency mode of the adsorbate [22]. This is obtained through the assumption that the velocity autocorrelation function can be written as

$$\langle v_{\mathbf{K}}(t)v_{\mathbf{K}}(0)\rangle = \langle v_{\mathbf{K}}^2\rangle e^{-\frac{t}{\tau_c}}\cos(\omega t + \delta) \tag{20}$$

for a corrugated surface potential, in comparison to (12) for a flat surface, in agreement with numerical simulations by Vega et al [23].

### 2.6 Memory Kernel

The integral over the kernel in (8) is known as the memory term [24], and equivalent to a filter in the time domain acting upon velocity [25].The same filter acts upon the white noise $\xi$ to give the coloured noise term $\zeta$:

$$\zeta = \int_{-\infty}^{t} \lambda(t-t')\xi(t')dt' \tag{21}$$

In the simplest case, $\lambda(t)$ may be written as a low pass filter, to remove excitations beyond a given frequency from the noise spectrum. This is described, in the time and frequency spectra, by:

$$\lambda(t) = \frac{1}{\tau}e^{\frac{t}{\tau}}, \qquad \left|\lambda(\omega)^2)\right| = \frac{1}{1+\tau^2\omega^2} \tag{22}$$

where the band limit of the noise is defined by a cut-off frequency, $\omega_c = 1/\tau$.

### 2.7 General Coloured Noise

As detailed by Avidor et al. [9], when considering a general form of the memory kernel:

$$\lambda(t) = \mathrm{Re}\Big\{\Sigma_k c_k e^{-t(\gamma k + i\omega k)}\Big\} \tag{23}$$

it is possible to rewrite Equation 8 in terms of the auxiliary momenta [26], such that:

$$\begin{pmatrix} \dot{p}(t) \\ \dot{\mathbf{s}}(t) \end{pmatrix} = \begin{pmatrix} -\nabla V'(x(t)) - \Sigma_{j\neq i}\mathbf{F}_{ij}(t) \\ \mathbf{0} \end{pmatrix} - \mathbf{A}\begin{pmatrix} p(t) \\ \mathbf{s}(t) \end{pmatrix} - \mathbf{B}\boldsymbol{\xi}(t) \tag{24}$$

where $p(t)$ is the conjugate momentum of $x(t)$, $s(t)$ is an $n$-elements vector with units of momentum and $\boldsymbol{\xi}(t)$ is a vector of $(n+1)$ Gaussian noise sources [27]. $\mathbf{A}$ and $\mathbf{B}$ are the drift and diffusion matrices respectively. Note that these equations of motion depend only on the current time $t$, and not the complete history of the particle.

The square matrices $\mathbf{A}$ and $\mathbf{B}$ with dimensions of length $(n+1)$ govern the dissipation and fluctuations, and can represent the filter applied in the friction kernel [28]. The fluctuation–dissipation theorem, requires that $\mathbf{A}$ and $\mathbf{B}$ are related by

$$mk_BT(\mathbf{A} + \mathbf{A}^T) = \mathbf{B}\mathbf{B}^T \tag{25}$$

The matrix $\mathbf{A}$ may be related to the memory kernel in (8) by [29]:

$$\lambda(t) = 2a_0\delta(t) - \mathbf{a}^T e^{-|t|\mathbf{A}'}\mathbf{a}' \tag{26}$$

where $\mathbf{A}$ is of the form:

$$\mathbf{A} = \begin{pmatrix} a_0 & \mathbf{a}^T \\ \mathbf{a}' & \mathbf{A}' \end{pmatrix} \tag{27}$$

Through consideration of the Fourier transform of (9):

$$\left\langle \zeta_i(\omega)\zeta_j(\omega') \right\rangle = \frac{mk_BT}{\sqrt{2\pi}}\lambda(\omega)\delta(\omega+\omega') \tag{28}$$

it can be seen that the power spectrum of the coloured noise is proportional to the Fourier transform of the memory kernel, $\lambda(\omega)$. Therefore, the noise can be filtered by suitable choice of memory kernel, which is defined through $\mathbf{A}$ according to (26).

### 2.8 Noise Filters

The primary filter used in this project was a low-pass noise filter. This gives an exponential decay in the memory kernel, which can be represented by the noise source spectral power density. This decay is characterised by the decay time $\tau$, so that $\lambda$ may be written as:

$$\lambda(t) = \frac{\gamma}{\tau}e^{-|t|/\tau}, \qquad \lambda(\omega) = \sqrt{\frac{2}{\pi}}\frac{\gamma}{1+(\tau\omega)^2} \tag{29}$$

where $\gamma$ denotes friction, and the memory kernel is defined my the matrix $\mathbf{A}$:

$$\mathbf{A} = \begin{pmatrix} 0 & -\sqrt{\gamma t} \\ \sqrt{\gamma t} & 1 \end{pmatrix} \tag{30}$$

# 3 Computational Methodology

## 3.1 PIGLE Software

PIGLE (Particles Interacting in Generalized Langevin Equation) [30] is software used to simulate the dynamics of multi species interacting particles responding to a 4D potential energy surface (3 spatial dimensions and one dimension for rigid body rotations), obeying to the generalized Langevin Equation. The potential energy surface should be periodic, and is implemented within a 'supercell', so that a particle's position is both recorded in space, and within the modular cell which corresponds to a unit cell in the surface structure.

Multiple species may be considered, with differing properties such as mass or friction. When the third spatial dimension ('z') is enabled, the user can choose either constant pressure (where desorbing particles re-appear at the system), or in simple mode where desorbing particles are being frozen for later filtration. However, this third dimension is not enabled for the simulations within this report, and the code is adapted to model one species only.

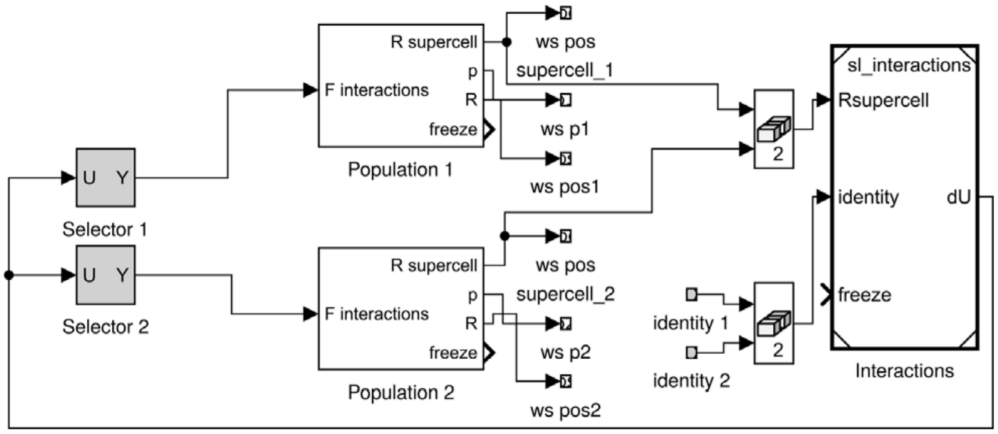


Figure 1: The top-level Simulink block of the PIGLE simulation. In each time-step, the Interactions block calculates and outputs the inter-adsorbate forces acting on all particles. Selector blocks select the force-information for all particles preassigned to a specific particle-population, which is then fed to the population dedicated Population blocks. Each Population block integrates the GLE for a single time-step and outputs the new momentum and position (total and super-cell relative), to the MATLAB workspace, and for calculation of inter-adsorbate forces. The position from all particle populations is combined and fed to the Interactions block, where the inter-adsorbate forces are computed for the next time-step. The inputs identity 1,2 to the Interactions block hold the identity (species) of each particle. Reproduced from [9].

The code is based in MATLAB, but uses the Simulink framework depicted in Figures 1 and 2 to optimise running efficiency. Simulink [31] is a package developed by Mathworks$^{TM}$ for simulations of time-dependent systems. The simulation code is represented in a block diagram in a graphical interface, with computational results transferred from output ports of one block (equivalent to a function) to the input ports of another.

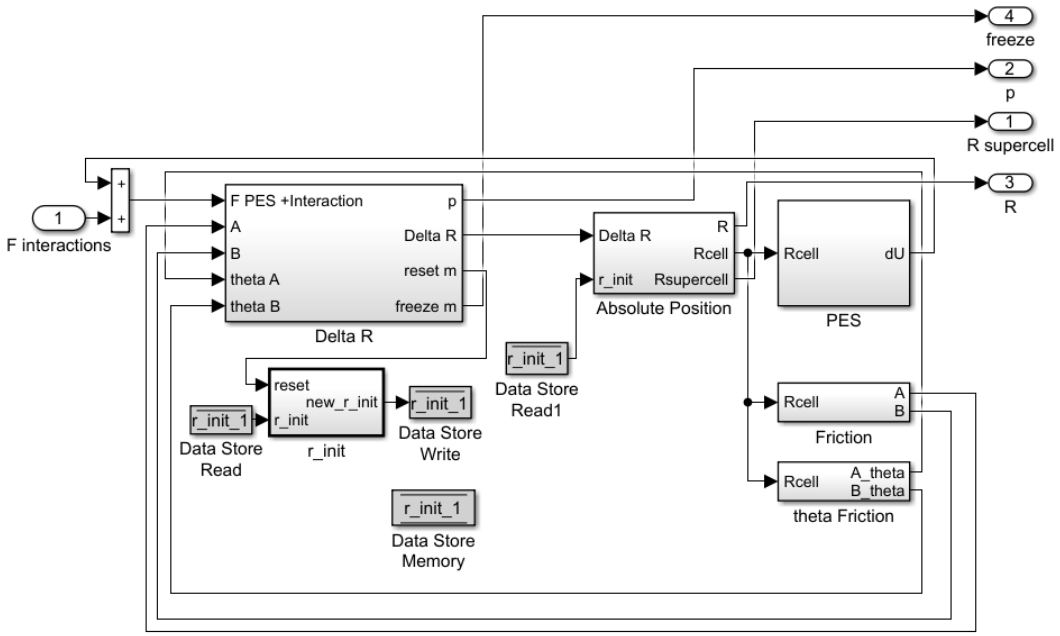


Figure 2: Block to compute the motion of population-specific particles. At each time-step, the inter adsorbate force on each particle is fed from the in-port, and is combined with the force resulting from the PES. The Delta R block then computes the momentum which is passed to an out-port, and the total change in translation/rotation which is passed to the Absolute Position block. It is there where the initial position is added to obtain the absolute position of each particle. The position within the simulation super-cell is calculated, and the two quantities are passed to out-ports. Position within the unit cell is also calculated, and is passed to the PES block for calculation of the PES-resulted force. Reproduced from [9].

### 3.2 Program Structure

Initially, the particles are assigned an arbitrary velocity from a thermal distribution corresponding to the simulation temperature, and randomly positioned about the simulation supercell. However, when a non-zero potential is applied, the random initial position of the particle may be unphysical (such as corresponding to a higher energy than the initial thermal distribution).

The program then allows for a 'thermalisation time', whereby particles in the system reach thermal equilibrium by dissipating through friction the excess energy corresponding to their initially unphysical position.

After this time point, the particles' trajectory is then recorded at pre-determined time steps, to obtain the ISF for each particle (and collectively). The individual particle scattering functions may be summed to give the coherent ISF, or a collective scattering function may be calculated from the average particle trajectory to give the incoherent scattering function [32]. While the coherent ISF tends to be measured experimentally, it is subject to greater random fluctuations and so the incoherent ISF is typically used in this report.

Within the simulation, there are two separate regimes separated by the friction time; this is the average time between collisions for a single particle, and is typically defined by the atomic coefficient of friction. On time scales smaller than this characteristic time, the particle moves ballistically as a result of the atomic collisions, whereas on longer time scales the net motion of the particle is diffusive. These two regions can both be observed in the ISF, with the steeper ballistic section commonly being referred to as the 'initial drop' [33].

### 3.3 Noise Filters

A summary of the filters implemented in PIGLE is given below in Table 1.

| Case Number | Filter Name | Description |
|---|---|---|
| 1 | None | Gaussian white noise source |
| 2 | Low-Pass | Frequencies above cut-off are damped exponentially |
| 3 | Spike | Selects frequencies in range of target frequency |
| 4 | Band Pass | Combination of Low- and High-Pass filters |
| 5 | Bi Low-Pass | Combination of two Low-Pass filters |

Table 1: The case numbers of different filters natively implemented in PIGLE

This is set on line 55 of *pigle_ui_surface_params*, and full details of filters applicable to this system are given by Ceriotti [29].

## 4 Results

### 4.1 Trajectory Characteristics

The distinctive random walk trajectory is dependant on a number of parameters, and a qualitative understanding of these relationships is instructive for further trajectory analysis. Figure 3 depicts a typical single particle random walk trajectory, and its dependence on temperature and friction. Figure 3b shows an increased temperature increasing the scaling of the trajectory, demonstrating the expected scaling of the Diffusion coefficient with temperature [34]. An increase in the atomic friction coefficient reduced the particle displacement under diffusion, and increases the noise in the trajectory (Figure 3c).

An external potential may also be applied to mimic the atomic surface, giving the trajectory observed in Figure 4. Note the scaling of the random walk is reduced compared to Figure 3b

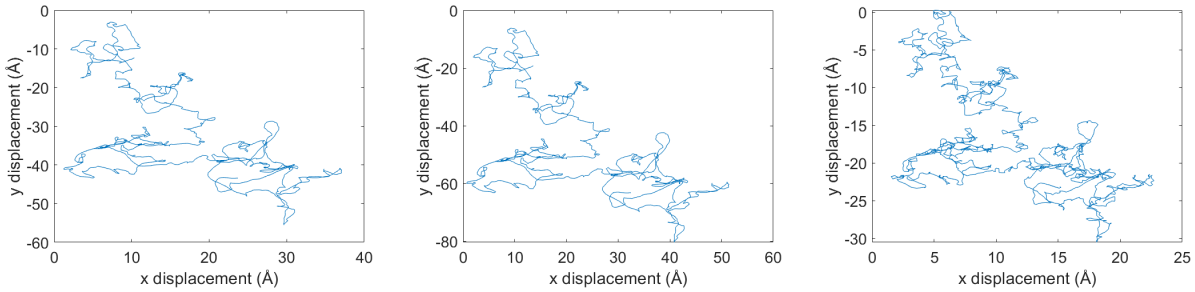


(a) Base Trajectory (b) $T = 280K$ (c) $\eta = 15ps^{-1}$

Figure 3: Single Particle trajectory (with no interaction forces in a zero potential) plotted over 100ps. Note the scaling of the random walk with increased temperature, and the increased noise at increased friction. All simulations at baseline parameters $m = 7amu, T = 140K, \eta = 5ps^{-1}$ unless otherwise stated, with a set seed for reproducibility.

(where all other parameters are the same), suggesting the particle is primarily confined to areas of lower potential and moves less freely.

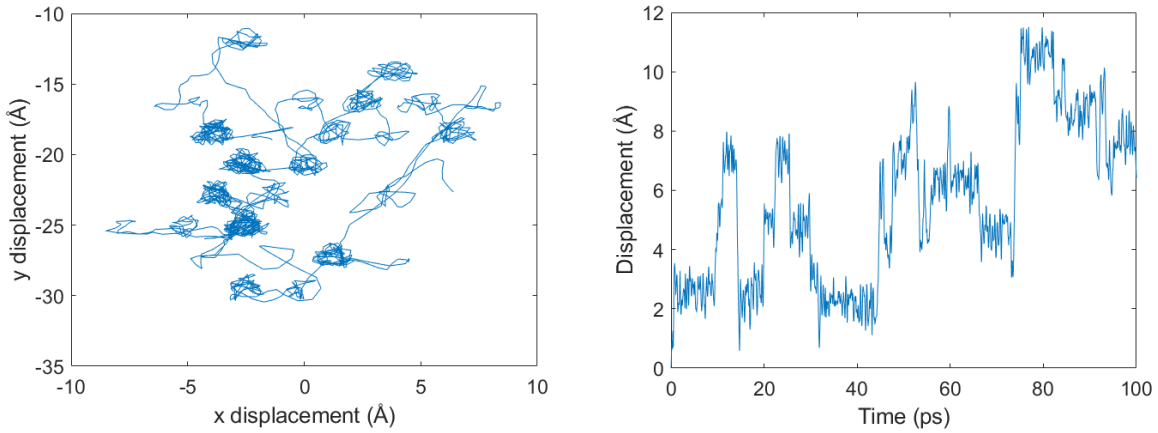


(a) Particle Trajectory (b) Displacement

Figure 4: Single particle trajectory for Li on a face centred cubic (FCC) potential surface, plotted over 100ps. Note the jumps between potential minima in (a), corresponding to sharp changes in the displacement in (b). Simulated with parameters $m = 7amu, T = 280K, \eta = 5ps^{-1}$, with a set seed for reproducibility.

This shows the distinctive 'jump diffusion', whereby a particle's primary motion across a surface is characterised by discrete 'jumps' (with a sharp change in the displacement magnitude in Figure 4b) between potential minima. The motion can also be visualised on a colourscale map of the potential surface (Figure 5), where the particle is clearly seen to favour the darker minima.

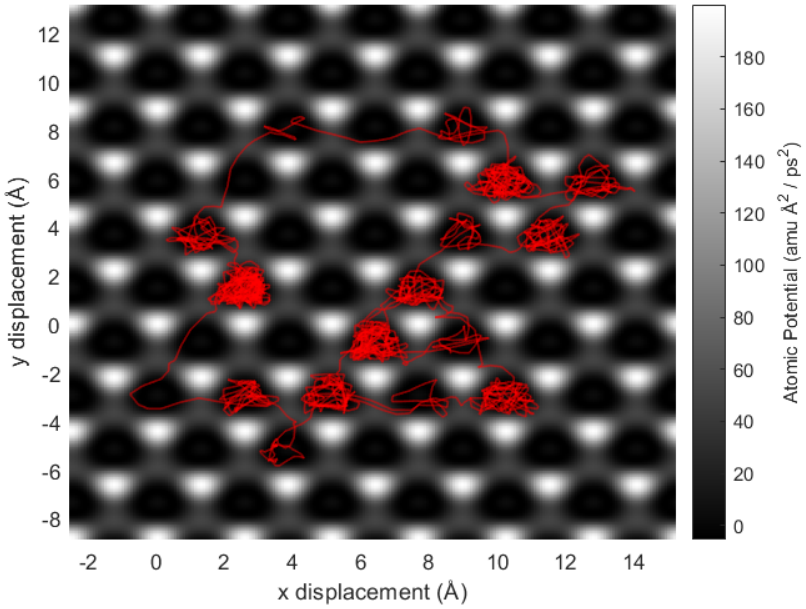


Figure 5: The trajectory of a Li particle on a FCC surface, over 100ps at 200K. The darker regions correspond to lower potential, and the lighter regions to higher potential, which the particle trajectory is depicted in red

### 4.2 ISF Characteristics

The ISF is used to characterise the temporal auto-correlation function over time, and is simulated here for comparison with experimental results from Helium spin echo spectroscopy. A single particle ISF is displayed in Figure 6 to illustrate the general characteristics.

Here the incoherent ISF is plotted, however this is the same as the coherent ISF for a single particle (and the coherent ISF averages to the incoherent ISF under a sufficient number of runs for any particle number). This plotted is replicated below with varied parameters in Figure 7.

Loss of coherence occurs faster when temperature is raised (Figure 7a), but slower when friction is raised (Figure 7b), due to the relative changes in particle mobility. Note that sections with a negative ISF are unphysical, and a statistical artefact, but are removed with greater sampling.

The effect of a potential surface may also be observed (Figure 8); note this introduces an oscillatory factor into the ISF, corresponding to motion over a periodic surface. This also reduced the decay of the ISF, as particles tend to be confined to potential minima on the surface, and so remain correlated for for greater lengths of time.

### 4.3 Effects of Coloured Noise

In its simplest form, coloured noise may be applied through the application of a low-pass filter to a white noise source, to remove the higher frequency components. The effect of this is clearly

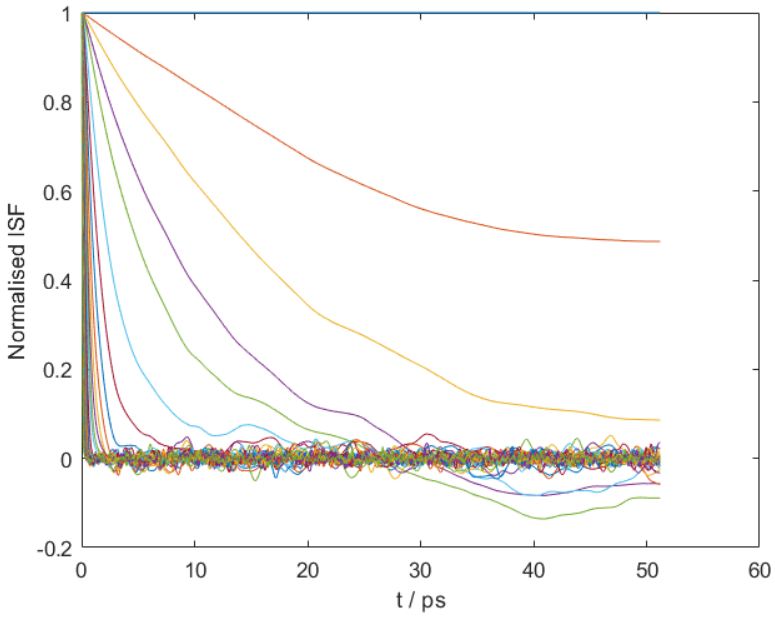


Figure 6: The incoherent ISF for a single Li particle on a zero potential surface, averaged over 100 runs. Simulated with parameters $m = 7amu, T = 140K, \eta = 5ps^{-1}$, for a range of $\Delta K$ between 0 and $5\mathring{A}^{-1}$.

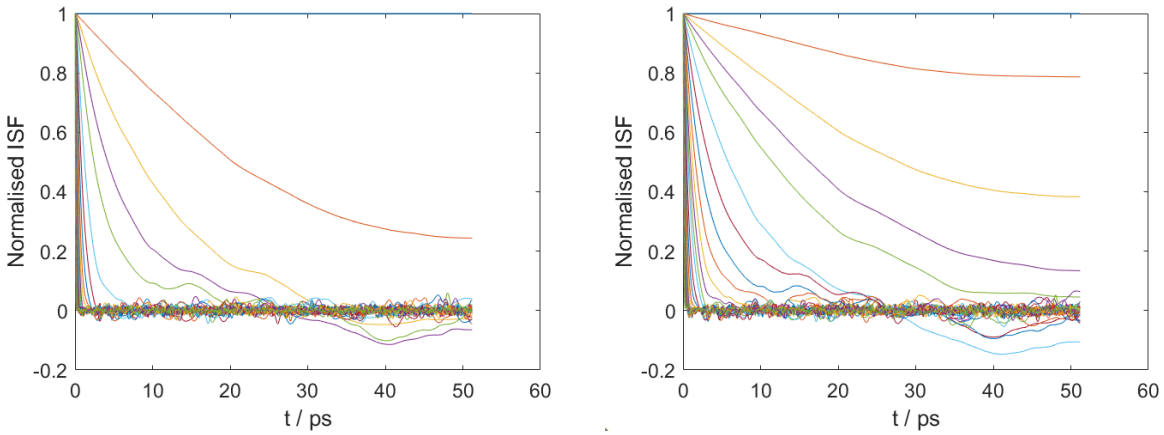


(a) $T = 280K$ (b) $\eta = 15ps^{-1}$

Figure 7: Single Particle ISF (with no interaction forces in a zero potential), averaged over 100 runs. Note faster decay with increased temperature, and the slower decay at increased friction. All simulations at baseline parameters $m = 7amu, T = 140K, \eta = 5ps^{-1}$ unless otherwise stated, with a set seed for reproducibility.

visualised in the trajectories in Figure 9, where the higher frequency components of motion are 'smoothed out' as the value of $\tau$ (corresponding to the cut-off frequency) is increased. This is also observed when a potential is applied, with the same smoothing of the trajectory within the potential wells.

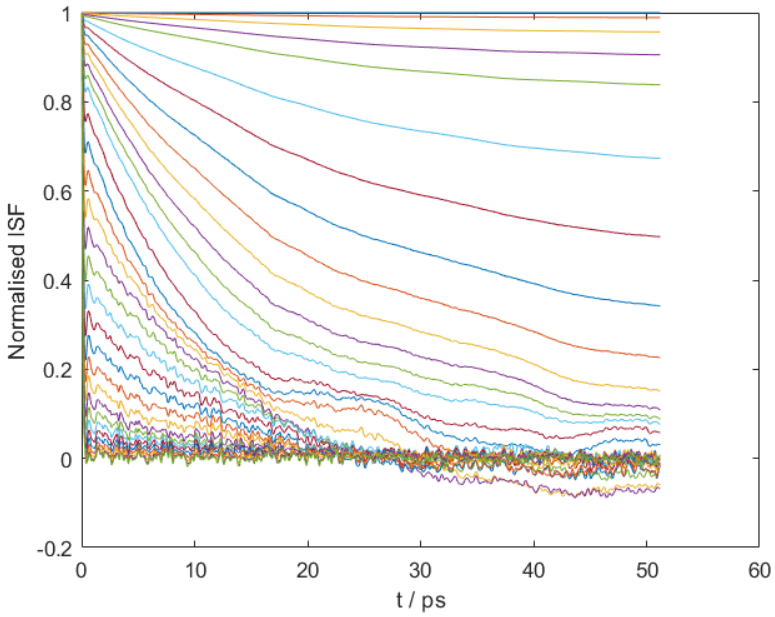


Figure 8: The incoherent ISF for a single Li particle on a FCC surface, averaged over 100 runs. Simulated with parameters $m = 7amu, T = 140K, \eta = 5ps^{-1}$, for a range of $\Delta K$ between 0 and $5\mathring{A}^{-1}$.

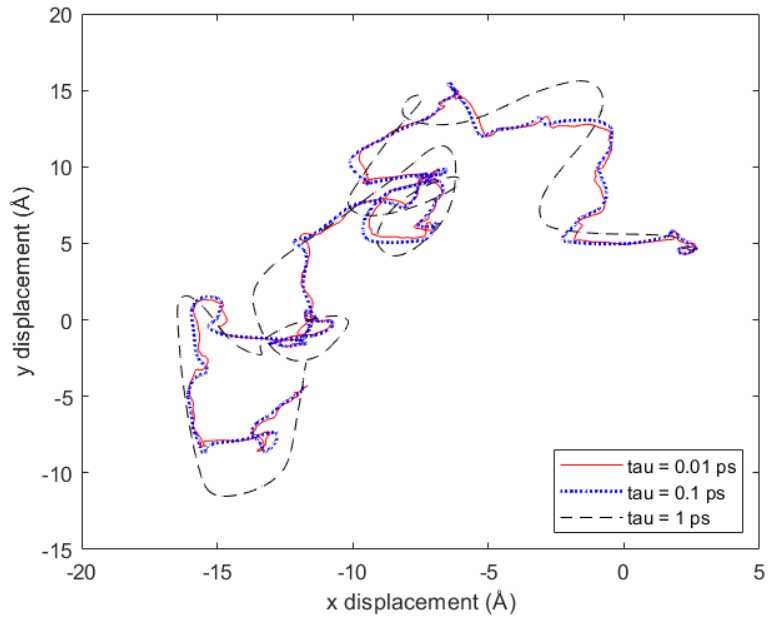


Figure 9: The trajectory of a Li particle on a zero potential surface, over 100ps. Note the removal of high frequency aspects to the trajectory when the cut-off time $\tau$ is increased.

It is instructive to consider the noise spectrum associated with this trajectory. As detailed in (8), a stochastic force acts upon the particle, and a histogram of the magnitude of these terms is given

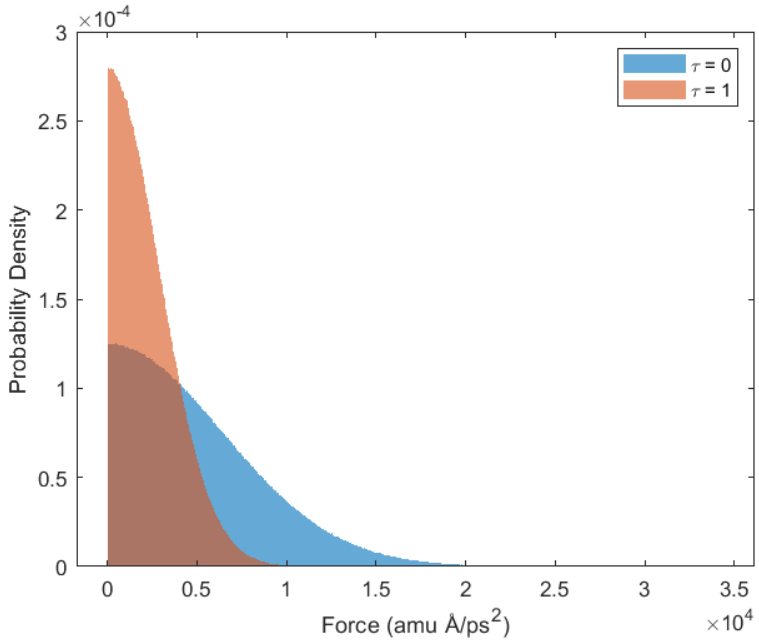


Figure 10: The probability density function of the stochastic force taking a particular magnitude. Note the suppression of higher values when a noise filter ($\tau = 1$) is applied.

in Figure 10, where it is clear that greater magnitude forces are suppressed when a noise filter is applied.

It is also observed, however, that a transition in the noise spectrum occurs at $\tau = 1/\gamma$, where the filtered noise takes the same spectrum as the unfiltered noise. For values of $\tau$ below this, the greater magnitude forces are augmented in the filtered noise, despite the filter still being classed as a low-pass filter. The physical explanation of this is not immediately obvious, and warrants further investigation.

In addition to this effect, it is worth noting that the trajectory of a particle in a GLE simulation does not tend to that of a particle in an LE simulation when the cut-off time $\tau$ is reduced to zero, despite the seed being constant in both cases. This may, however, be due to different uses of the seed within these simulations, as both trajectories had approximately the same characteristics. The ISFs recorded in both cases were similar to within noise variation, however it was not possible to characterise this further.

We may also consider the more general effect of a noise filter on the ISF, as depicted in Figure 11. The characteristic form of the ISF is similar, however the decay occurs faster when a noise filter is applied, in accordance with the analytic solutions to the LE and GLE respectively. This may be attributed to the removal of small, high frequency fluctuations, so the particle is more likely to continue along a constant line of motion away from its initial point, reducing its temporal autocorrelation function.

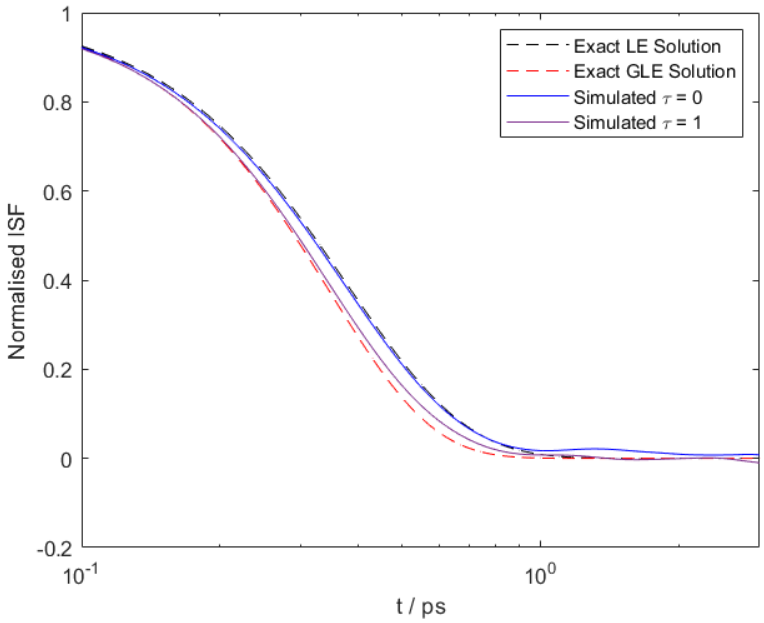


Figure 11: The incoherent ISF for a single Li particle on a zero potential surface, averaged over 100 particles, with and without a low-pass noise filter applied (characterised by cut-off time $\tau$). Simulated with parameters $m = 7amu, T = 140K, \eta = 5ps^{-1}, \Delta K = 1\mathring{A}^{-1}$.

It should be noted that each ISF is normalised separately to its own maximum. In previous literature (Figure 5.18 of [35]), these were normalised relative to their long-time behaviour, however the ISFs did not tend to a steady state value in the simulations I present, but oscillated about zero. However the general trends and line-shape observed by Ward are indeed replicated here, and this noise can be reduced by sampling over longer time scales than the ISF is plotted over.

### 4.4 Ballistic and Diffusive Regions

As described in Section 3.2, there are two characteristic regimes; the short time (ballistic) regime and the long time (diffusive) regime. Here, the ISFs for both regimes are simulated and contrasted.

The exact solution for the ISF (14) suggests a short time approximation of a Gaussian form, given in (16). Therefore in the ballistic region we may fit to a general Gaussian of the form:

$$I(\mathbf{K}, t) = Ae^{-\frac{t^2}{2\sigma^2}} \tag{31}$$

where $A$ and $\sigma$ are fitting parameters, so that $\mathbf{K}$ and $1/\sigma$ should be linearly proportional. This linear relationship is characteristic of a gas of quantum particles undergoing ballistic motion [36].

The constant of proportionality is given by $\sqrt{D/\tau}$, which is equal to $\sqrt{\langle v_{\mathbf{K}}^2 \rangle} = \sqrt{k_B T/m}$ according

to (15). This has a theoretical value of $4.078\mathring{A}$, in agreement with the statistical gradient of $4.058 \pm 0.03\mathring{A}$ (given by the linear best fit line calculated from least-squares regression).

This linear relationship is validated in Figure 12, where the simulated data is shown to fit the linear trend well beyond approximately 1 ps. It should also be noted that this gradient is only dependant on the temperature of the system and the mass of the particle, and so is unaffected by the the low-pass filter applied in the $\tau = 1$ case.

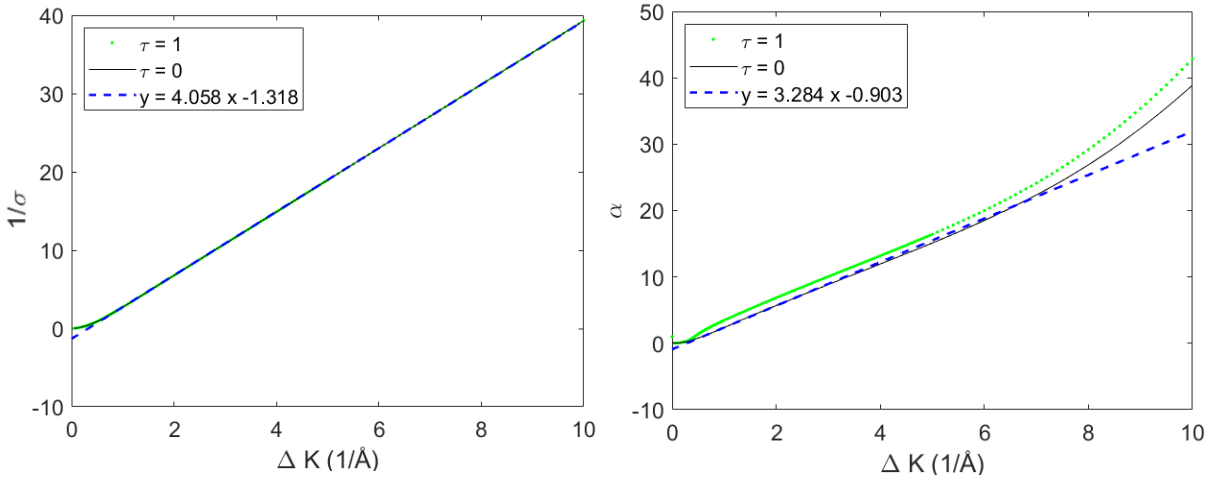


(a) Ballistic Region (20ps)

(b) Diffusive Region (100ps)

Figure 12: Fitting parameters $\alpha$ and $\sigma$ plotted over $\mathbf{\Delta K}$ for a single particle ISF, with a zero potential and averaged over 100 runs. Note the strong agreement with the linear prediction beyond 1ps in the ballistic case, and more significant quadratic term in the diffusive case. All simulations at baseline parameters $m = 7amu, T = 140K, \eta = 5ps^{-1}$, with a set seed for reproducibility.

The diffusive case was instead fitted to an exponential decay, of the form:

$$I(\mathbf{K}, t) = Ae^{-\alpha t} + B \tag{32}$$

where $A$, $B$ and $\alpha$ are fitting parameters. This shows a greater distinction between the unfiltered and filtered cases, with a lower linear component. The most significant difference is the quadratic component at higher $\Delta K$ values; this becomes more significant over longer time scales (such as 1ns) which are more commonly considered diffusive. A shorter timescale was, however, chosen here for ease of comparison and plotting, while still drawing attention to the key features.

### 4.5 Application of a Potential

The main focus of this report is to combine the noise spectrum analysis with a potential surface, utilising the potential of the PIGLE software. The Cu (111) surface is chosen as an initial candidate for consideration on this surface, due to its experimental prevalence and relevance [37], as well as our detailed knowledge of the structure of this system [38].

The maxima in energy was taken as $45eV$, corresponding to the height of the top site. This has little physical relevance in the simulation however, as diffusion primarily occurs via the HCP (hexagonally close packed) and FFC (face centred cubic) sites, over the saddle point denoted by the red line in Figure 13. The activation energy of this transition is given as $9eV$, in agreement with [35], while the intermediate slope energies were set at $13eV$.

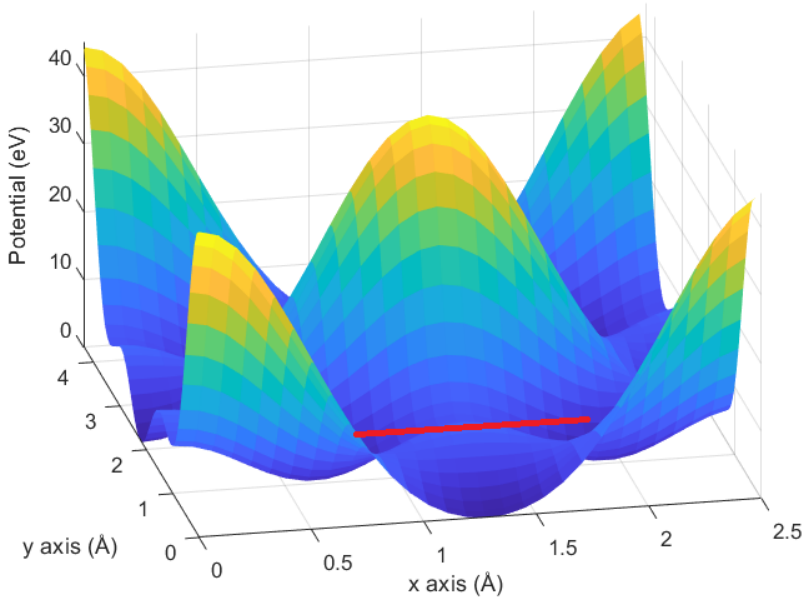


Figure 13: The potential energy surface for Cu (111), given over a single unit cell of dimensions $2.56\mathring{A} \times 4.43\mathring{A}$. The line in red demonstrates the path across the saddle point, which is the preferred route for diffusion.

This surface has a relatively weak interaction potential, and so does not affect the trajectory of the particle to the extent observed in Figure 5, however the differences are more significant in the ISF (where the decay is again reduced due to the increased temporal correlation of the particle).

The ISFs with and without the application of a low-pass filter are shown are Figure 14. The analytic solutions (in the case of no potential) to the LE (given in (14)) and the GLE (given in (17)) are depicted for comparison, and display remarkable agreement with the zero-potential simulations, especially over shorter timescales.

Again the application of a potential surface increases the decay time of the ISF, particularly at longer timescales. This is due to the effect of the potential minima observed in Figure 4, where particles become trapped in potential wells, so their movement is better characterised by jump diffusion with periods of relative stationarity.

The effect of the magnified potential is particularly pronounced, and the fluctuations visible in Figure 14b demonstrate this as they correspond to movement within a potential well (where the particle may move back and forth relative to its initial position). This is more significant where

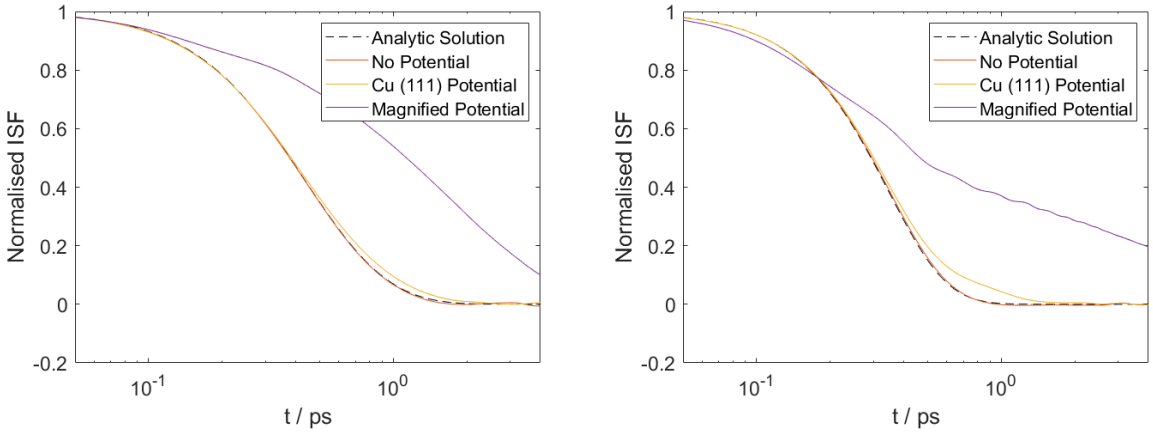


(a) White Noise ($\tau = 0$)

(b) Low Pass Filter ($\tau = 1$)

Figure 14: Single Particle ISF, averaged over 25 runs of 25 particles each using baseline parameters. There is a comparison to the analytic forms of the solutions to the LE and GLE respectively, and simulations with a Cu (111) potential applied, and a strengthened potential where the standard Cu (111) potential is magnified by a factor of 10.

such movement is more pronounced due to the removal of random, high-frequency fluctuations, and may correspond to regular motion within the potential well.

### 4.6 Experimental Fitting

With the use of the potential energy surface (PES) developed in Section 4.5, we may replicate the plots of fitting parameter $\alpha$ against $\Delta K$ given in Figure 12. This enabled comparison with experimental data obtained by Ward [35].

Initially the friction and PES were optimised to match the long time diffusive motion of the particle, with the comparison between experimental and theoretical data given in Figure 15a. Here the fitting parameter is the decay time from a single exponential decay with a background constant, as given in (32).

A saddle point activation energy of $8eV$ was used, with an atomic coefficient of friction of $1ps^{-1}$ to achieve this fit with the simulated values in the diffusive region. A low-pass noise filter was subsequently added, with the cut-off parameter $\tau$ to be optimised for agreement with the experimental data in the ballistic region, given in Figure 15b.

To consider this faster ballistic decay, the fitted primary exponential decay curves are subtracted from the simulated ISF data. The residual ISF is then fitted to the equation:

$$I(\mathbf{K}, t) = Ce^{-\alpha_2 t} + De^{-\frac{t^2}{2\sigma^2}} \tag{33}$$

where $\alpha_2$ characterises the faster ballistic exponential decay. The primary exponential fit is ap-

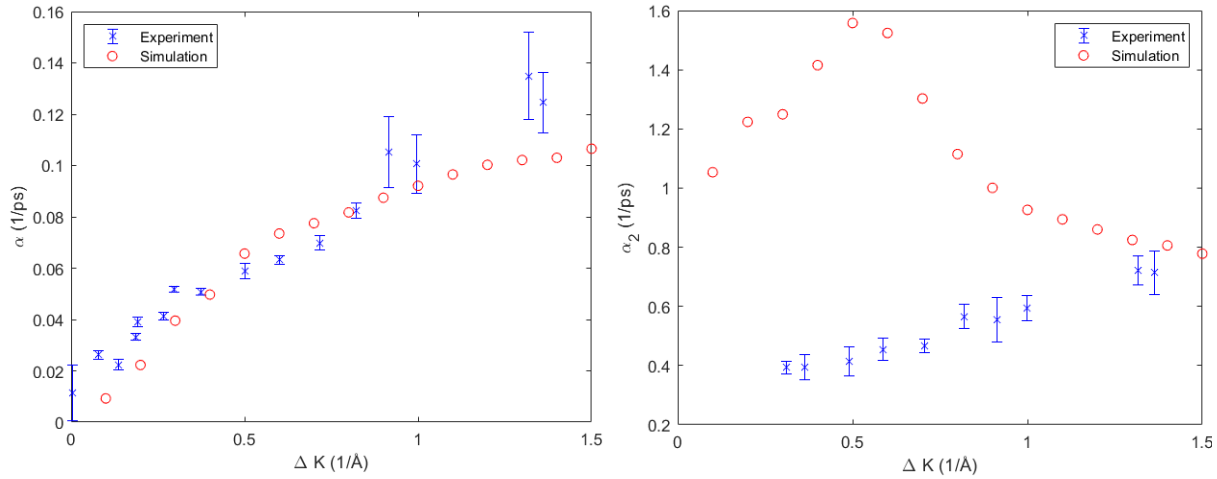


(a) Primary Exponential Decay

(b) Faster Ballistic Decay

Figure 15: Fitting parameters $\alpha$ and $\alpha_2$ plotted over $\mathbf{\Delta K}$ for a single particle ISF (over $800ps$, sampled at $10fs$ intervals), with a Cu (111) potential and averaged over 25 particles. All simulations at baseline parameters $m = 7amu, T = 140K, \eta = 1ps^{-1}$, with a set seed for reproducibility.

proached iteratively, ensuring a good fit at longer time scales before increasing the time range considered to include smaller values of $t$ while maintaining the same level of agreement. A cut-off parameter of $\tau = 0.8ps^{-1}$ was chosen, however it proved difficult to obtain a fit in good agreement with the experimental data in Figure 15b.

The double exponential decay is particularly prominent in the ISF for greater $\Delta K$ values depicted in Figure 16, where a local minima is observed between decays. However, 'kinks' in the ISF curves at lower values of $\Delta K$ enabled consistent analysis of all curves within this experimental range. It is worth noting that these features tend to be characteristic of higher friction regimes, where they tend to be more dominant, and correspond to the different scales of jump diffusion across the surface.

## 5 Conclusion

The effect of varying parameters (particularly the cut-off noise filter) was demonstrated on particle trajectories, and the results ISFs were in agreement with the analytic lineshapes. When fitting the ballistic ISF to a general Gaussian, the wavevector $\mathbf{K}$ and the inverse of the standard deviation $\sigma$ should be directly proportional, with this constant of proportionality given by $\sqrt{k_B T/m}$ according to (15). This has a theoretical value of $4.078\mathring{A}$, which was in agreement with the statistical gradient of $4.058 \pm 0.03\mathring{A}$ (given by the linear best fit line calculated from least-squares regression).

A potential energy surface was introduced to allow comparison to experimental data; in this report Li diffusion on a Cu (111) surface is considered. This allows observation of the characteristic jump diffusion motion typical in a corrugated potential surface, and tends to prolong the ISF decay as

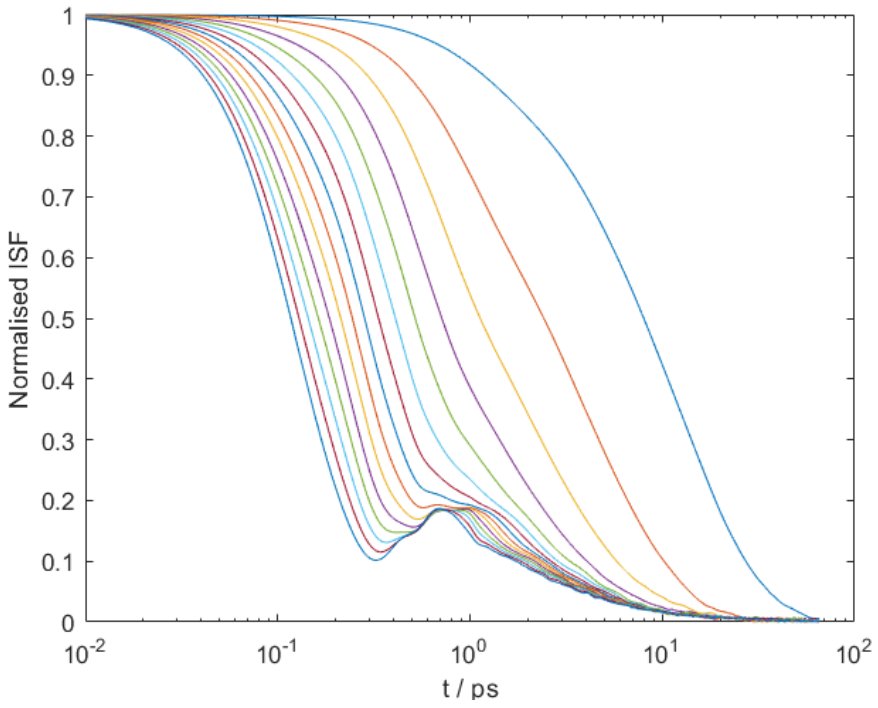


Figure 16: Single particle incoherent ISF, plotted over $80ps$ with sampling at $1fs$ intervals. Averaged over 1000 Li particles subject to a Cu (111) potential, over a range of $\mathbf{\Delta K}$ from $0.1 - 1.5\mathring{A}^{-1}$, and at baseline parameters $m = 7amu, T = 140K, \eta = 1ps^{-1}, \tau = 0.8ps^{-1}$.

the particles remain confined to individual minima on the PES for extended periods of time.

A noise filter is also utilised to remove unphysical, high frequency impulses present in the random noise spectrum. This allows greater agreement with experimental data in Section 4.6, however the low pass filter alone is insufficient to replicate the experimental trends observed. It is suggested that more advanced filters are utilised to replicate the phonon spectrum of the metal surface more accurately, in order to achieve better agreement with the experimental data.

## References


[1]G. Alexandrowicz and A. P. Jardine, "Helium spin-echo spectroscopy: studying surface dynamics with ultra-high-energy resolution", Journal of Physics: Condensed Matter **19**, 305001 (2007).

[2]A. Jardine, H. Hedgeland, G. Alexandrowicz, W. Allison, and J. Ellis, "Helium-3 spin-echo: principles and application to dynamics at surfaces", Progress in Surface Science **84**, 323–379 (2009).

[3]A. P. Jardine, E. Y. M. Lee, D. J. Ward, G. Alexandrowicz, H. Hedgeland, W. Allison, J. Ellis, and E. Pollak, "Determination of the quantum contribution to the activated motion of hydrogen on a metal surface: H/Pt(111)", Physical Review Letters **105**, 10.1103/physrevlett.105.136101 (2010).

[4]H. Hedgeland, P. R. Kole, H. R. Davies, A. P. Jardine, G. Alexandrowicz, W. Allison, J. Ellis, G. Fratesi, and G. P. Brivio, "Surface dynamics and friction of K/Cu(001) characterized by helium-3 spin-echo and density functional theory", Physical Review B **80**, 10.1103/physrevb.80.125426 (2009).

[5]I. Langmuir, "The electron emission from thoriated tungsten filaments", Physical Review **22**, 357–398 (1923).

[6]R. Kissel-Osterrieder, F. Behrendt, and J. Warnatz, "Dynamic monte carlo simulations of catalytic surface reactions", Proceedings of the Combustion Institute **28**, 1323–1330 (2000).

[7]M. Andersen, C. Panosetti, and K. Reuter, "A practical guide to surface kinetic monte carlo simulations", Frontiers in Chemistry **7**, 10.3389/fchem.2019.00202 (2019).

[8]M. Diamant, S. Rahav, R. Ferrando, and G. Alexandrowicz, "Interpretation of surface diffusion data with langevin simulations: a quantitative assessment", Journal of Physics: Condensed Matter **27**, 125008 (2015).

[9]N. Avidor, P. Townsend, D. Ward, A. Jardine, J. Ellis, and W. Allison, "PIGLE — particles interacting in generalized langevin equation simulator", Computer Physics Communications **242**, 145–152 (2019).

[10]G. Box, *Time series analysis : forecasting and control* (Prentice Hall, Englewood Cliffs, N.J, 1994).

[11]P. Langevin, "Sur la théorie du mouvement brownien", Comptes rendus de l'Académie des Sciences **146**, 530–533 (1908).

[12]G. Stokes, "On the effect of internal friction of fluids on the motion of pendulums", Transactions of the Cambridge Philosophical Society **9**, 8–106 (1851).

[13]A. Khintchine, "Korrelationstheorie der stationären stochastischen prozesse", Mathematische Annalen **109**, 604–615 (1934).

[14]P. Gagniuc, *Markov chains : from theory to implementation and experimentation* (John Wiley & Sons, Hoboken, NJ, 2017).

[15]R. Kubo, "The fluctuation-dissipation theorem", Reports on Progress in Physics **29**, 255–284 (1966).

[16]J. L. Vega, R. Guantes, and S. Miret-Artés, "Quasielastic and low vibrational lineshapes in atom–surface diffusion", Journal of Physics: Condensed Matter **16**, S2879–S2894 (2004).

[17]C. T. Chudley and R. J. Elliott, "Neutron scattering from a liquid on a jump diffusion model", Proceedings of the Physical Society **77**, 353–361 (1961).

[18]J. L. Doob, "The Brownian Movement and Stochastic Equations", Annals of Mathematics **43**, 351–369 (1942).

[19]R. Kubo, M. Toda, and N. Hashitsume, "Statistical mechanics of linear response", in *Statistical physics II* (Springer Berlin Heidelberg, 1991), pp. 146–202.

[20]P. S. M. Townsend and D. J. Ward, "The intermediate scattering function for quasi-elastic scattering in the presence of memory friction", (2018).

[21]R. Martinez-Casado, J. L. Vega, A. S. Sanz, and S. Miret-Artes, "Generalized chudley-elliott vibration-jump model in activated atom surface diffusion", The Journal of Chemical Physics **126**, 194711 (2007).

[22]J. Braun, A. P. Graham, F. Hofmann, W. Silvestri, J. P. Toennies, and G. Witte, "A he-atom scattering study of the frustrated translational mode of CO chemisorbed on defects on copper surfaces", The Journal of Chemical Physics **105**, 3258–3263 (1996).

[23]J. L. Vega, R. Guantes, and S. Miret-Artes, "Chaos and transport properties of adatoms on solid surfaces", Journal of Physics: Condensed Matter **14**, 6191–6232 (2002).

[24]R. Zwanzig, *Nonequilibrium statistical mechanics* (Oxford University Press, Oxford New York, 2001).

[25]R. Martinez-Casado, A. Sanz, J. Vega, G. Rojas-Lorenzo, and S. Miret-Artés, "Linear response theory of activated surface diffusion with interacting adsorbates", Chemical Physics **370**, 180–193 (2010).

[26]F. Marchesoni and P. Grigolini, "On the extension of the kramers theory of chemical relaxation to the case of nonwhite noise", The Journal of Chemical Physics **78**, 6287–6298 (1983).

[27]J. Łuczka, "Non-markovian stochastic processes: colored noise", Chaos: An Interdisciplinary Journal of Nonlinear Science **15**, 026107 (2005).

[28]M. Ceriotti, G. Bussi, and M. Parrinello, "Langevin equation with colored noise for constant-temperature molecular dynamics simulations", Physical Review Letters **102**, `10.1103/physrevlett.102.020601` (2009).

[29]M. Ceriotti, "A novel framework for enhanced molecular dynamics based on the generalized langevin equation", en, PhD thesis (2010).

[30]N. Avidor, *Na364/pigle v1.0.0-beta2*, 2018.

[31]M. SIMULINK, "Version 2009", SimPowerSystem, One quadrant chopper DC drive.

[32]K. Sköld, J. M. Rowe, G. Ostrowski, and P. D. Randolph, "Coherent- and incoherent-scattering laws of liquid argon", Physical Review A **6**, 1107–1131 (1972).

[33]R. Guerra, U. Tartaglino, A. Vanossi, and E. Tosatti, "Ballistic nanofriction", Nature Materials **9**, 634–637 (2010).

[34]A. Einstein, "Uber die von der molekularkinetischen theorie der wärme geforderte bewegung von in ruhenden flüssigkeiten suspendierten teilchen", Annalen der Physik **322**, 549–560 (1905).

[35]D. Ward, "A study of spin-echo lineshapes in helium atom scattering from adsorbates" (University of Cambridge, 2013).

[36]P. S. M. Townsend and A. W. Chin, "Intermediate scattering function and quantum recoil in non-markovian quantum diffusion", Physical Review A **98**, 10.1103/physreva.98.022106 (2018).

[37]V. Higgs, P. Hollins, M. Pemble, and J. Pritchard, "Formation of a surface nitride on copper(111) and its influence on carbon monoxide adsorption: investigation by leed, RAIRS and EELS.", in *Vibrations at surfaces 1985, proceedings of the fourth international conference* (Elsevier, 1986), pp. 137–144.

[38]S. J. Gurman, "Surface states and the surface potential: the copper (111) face", Journal of Physics C: Solid State Physics **9**, L609–L613 (1976).